Mesyl phosphoramidate backbone modified antisense oligonucleotides targeting miR-21 with enhanced in vivo therapeutic potency

Olga A. Patutina (Ольга Патутина)[a,1], Svetlana K. Gaponova (Miroshnichenko) (Светлана Гапонова)[a,1], Aleksandra V. Sen'kova (Александра Сенькова)[a], Innokenty A. Savin (Иннокентий Савин)[a], Daniil V. Gladkikh (Даниил Гладких)[a], Ekaterine A. Burakova (Екатерина Буракова)[b,c], Alesya A. Fokina (Алеся Фокина)[b,c], Mikhail A. Maslov (Михаил Маслов)[d] (ORCID), Elena V. Shmendel' (Елена Шмендель)[d], Mattew J. A. Wood[e], Valentin V. Vlassov (Валентин Влассов)[a], Sidney Altman[f,g,2] (ORCID), Dmitry A. Stetsenko (Дмитрий Стеценко)[b,c], and Marina A. Zenkova (Марина Зенкова)[a,2]

[a]Laboratory of Nucleic Acids Biochemistry, Institute of Chemical Biology and Fundamental Medicine, Siberian Branch of the Russian Academy of Sciences, 630090 Novosibirsk, Russia; [b]Department of Physics, Novosibirsk State University, 630090 Novosibirsk, Russia; [c]Sector of Plant Chemical Biology, Institute of Cytology and Genetics, Siberian Branch of the Russian Academy of Sciences, 630090 Novosibirsk, Russia; [d]Department of Chemistry and Technology of Biologically Active Compounds, Medical and Organic Chemistry Named after N. A. Preobrazhensky, Moscow Institute of Radio Engineering, Electronics and Automation–Russian Technological University, 119454 Moscow, Russia; [e]Department of Paediatrics, University of Oxford, OX3 9DU Oxford, United Kingdom; [f]Department of Molecular, Cellular and Developmental Biology, Yale University, New Haven, CT 06520-8103; and [g]Life Sciences Division, Arizona State University, Tempe, AZ 85287-4501

The design of modified oligonucleotides that combine in one molecule several therapeutically beneficial properties still poses a major challenge. Recently a new type of modified mesyl phosphoramidate (or μ-) oligonucleotide was described that demonstrates high affinity to RNA, exceptional nuclease resistance, efficient recruitment of RNase H, and potent inhibition of key carcinogenesis processes in vitro. Herein, using a xenograft mouse tumor model, it was demonstrated that microRNA miR-21–targeted μ-oligonucleotides administered in complex with folate-containing liposomes dramatically inhibit primary tumor growth via long-term down-regulation of miR-21 in tumors and increase in biosynthesis of miR-21–regulated tumor suppressor proteins. This antitumoral effect is superior to the effect of the corresponding phosphorothioate. Peritumoral administration of μ-oligonucleotide results in its rapid distribution and efficient accumulation in the tumor. Blood biochemistry and morphometric studies of internal organs revealed no pronounced toxicity of μ-oligonucleotides. This new oligonucleotide class provides a powerful tool for antisense technology.

antisense oligonucleotide | DNA modification | mesyl oligonucleotide | oncogenic microRNA | phosphorothioate

Antisense-based RNA targeting approaches laid the foundation for one of the powerful drug discovery platforms (1). Antisense oligonucleotides (ASOs) are short synthetic nucleic acids designed to inhibit the expression of target RNA by sequence-specific recognition.

The first generation modified ASOs are well-known phosphorothioate oligodeoxynucleotides (PS ASOs) (1, 2). Despite decades of efforts, no other modification has been developed combining a number of important properties, such as high nuclease resistance, the ability to recruit RNase H, and enhanced protein binding facilitating ASOs uptake by the cells and accumulation in peripheral tissues (3). The PS modification currently forms the backbone of the main ASOs in clinical trials, combined with other modifications of the second or third generation, such as 2′-O-methoxyethyl (MOE), locked nucleic acid (LNA), or constrained ethyl (cEt), stabilizing duplex interactions (the gapmer oligonucleotides) (2). Despite the number of benefits, one of the significant drawbacks of PS ASOs that limit its clinical utility is substantial toxicity (4–7). It was shown that toxicity of some MOE, LNA, or cEt PS gapmer ASOs arises from enhanced binding to cellular proteins, resulting in RNase H1-dependent nucleolar mislocalization of paraspeckle proteins,

nucleolar stress and fragmentation, up-regulation of P21, and activation of caspases, leading to large-scale apoptosis (4, 5, 8).

To improve clinical performance of oligonucleotides, attempts are made to design hybrid molecules that combine in one structure several modifications. However, the preparation of mixmers complicates synthesis and increases the cost of such compounds. Design of new modified oligonucleotides that would combine in one oligomer the maximum number of therapeutic capabilities remains as relevant as ever.

Oligodeoxynucleotides containing an aromatic sulfonyl phosphoramidate group were first obtained over a decade ago but never studied as potential antisense compounds (9). Recently, we synthesized oligodeoxynucleotides with the tosyl phosphoramidate group and showed that their duplex with RNA was destabilized relative to the native DNA:RNA duplex, presumably due to the bulkiness of the tosyl group at the internucleotidic position (10). This has prompted us to investigate a novel DNA analog that

Significance

Sequence-specific targeting of disease-associated RNAs by new types of chemically modified antisense oligonucleotides with improved physicochemical and biological properties is still in high demand. miRNA-addressing mesyl phosphoramidate oligonucleotides represent prospective therapeutics since they reveal good bioavailability in tumor tissue, potent and long-lasting antitumor effect, high targeted specificity associated with reactivation of tumor suppressor proteins, and physiological safety.

incorporates the mesyl (methanesulfonyl) phosphoramidate group (μ-modification), which has the smallest one-carbon side chain (Fig. 1). Oligodeoxynucleotides with a few μ-groups replacing the phosphodiester (PO) group indeed showed improved RNA binding over tosyl analogs (11). Next, ASOs substituting μ-modifications for natural PO groups at every internucleotidic position were designed to inhibit oncogenic microRNAs (miRNAs) (12), in particular, miR-21, which is recognized as a potent oncogene and causes global dysregulation of gene expression in malignant cells (13–17). μ-oligonucleotides demonstrated high affinity to RNA, exceptional resistance to nucleases, and potent recruitment of RNase H, with increased efficiency of catalytic miRNA degradation as compared to PS ASOs. The biological potential of μ ASOs was shown in cell culture and contributes to the efficient and specific inhibition of key carcinogenic processes in vitro (12). The present investigation focuses on the study of therapeutically important characteristics of the miR-21–targeted μ ASOs as potential antitumor agents in vivo: biodistribution, specific and off-target effects, kinetics of tumor suppression, and assessment of the main criteria of systemic toxicity. Herein, the enhanced in vivo potency of μ ASOs compared with PS ASOs indicates that this oligonucleotide class represents a highly-potent tool of antisense technology.

Results

Structure of Chemically Modified ASOs.
In this work, 22-mer oligodeoxyribonucleotides complementary to mature miR-21 (18) and containing μ- or PS-modifications of all internucleotide bonds, termed as μ-miR-21-ON and PS-miR-21-ON, respectively, were studied (for sequences and structures, see Fig. 1 and *Materials and Methods*). As a control, fully modified μ- or PS-scrambled oligodeoxyribonucleotides (μ-Scr-ON and PS-Scr-ON) of the same length, with a sequence that had no homology in the mammalian genome, were used.

Kinetics of miRNA Down-Regulation In Vitro by μ and PS ASOs.
To develop the optimal regimen of antisense therapy with μ ASOs in vivo, the kinetics of miRNA silencing by μ ASOs (100 nM) was investigated in melanoma B16 cells that combine the main malignant features—aggressiveness, rapid proliferation, and high metastatic potential. Lipofectamine 2000-mediated transfection of B16 cells with μ-miR-21-ON causes a 6-d-lasting decrease in the miR-21 level, with maximum down-regulation observed at 72 h (*SI Appendix*, Fig. S1). Similar kinetics of miRNA down-regulation was also evidenced for μ ASOs targeted to oncogenic miRNAs miR-155 and miR-17: The lowest level of miRNAs

Fig. 1. Structures and sequences of antisense oligonucleotides (ASOs) targeted to miR-21. (*A*) Structures of DNA phosphate group modifications: phosphodiester (PO), phosphorothioate (PS), and mesyl phosphoramidate (μ). (*B*) Sequences of oligonucleotides μ-miR-21-ON and PS-miR-21-ON used in the study. Indices μ and S stand for mesyl phosphoramidate group and phosphorothioate group, respectively.

accounting for an 80 to 90% decrease was reached by 72 h and was preserved up to 144 h (*SI Appendix*, Fig. S1). It should be emphasized that no unspecific down-regulation of other miRNAs, for instance, miR-155 and miR-17, was observed after cell treatment with μ-miR-21-ON (*SI Appendix*, Fig. S1). In turn, PS-miR-21-ON promoted no more than a twofold decrease in the level of miR-21 observed by 48 h, with the total duration of inhibition being less than 72 h (*SI Appendix*, Fig. S1).

Biodistribution of μ and PS ASOs in Tumor-Bearing Mice.
To study the biodistribution and therapeutic potential of μ ASOs, a xenograft model of human epidermoid carcinoma KB-8-5 cells in severe combined immunodeficient (SCID) mice was chosen. The use of this model permits one to assess a direct antitumor effect and minimize the interference of the immunity engagement in response to oligonucleotide therapy.

To study biodistribution and conduct an initial analysis of pharmacokinetic parameters of the developed oligonucleotides, KB-8-5 tumor-bearing SCID mice were peritumorally or intravenously (i.v.) injected with 40 μg of μ- or PS-Cy5.5–modified oligonucleotides. Folate-containing cationic liposomes F shown to efficiently deliver small interfering RNA (siRNA) to KB-8-5 tumors characterized by high abundance of folate receptors were used as a delivery vehicle (19).

Data analysis showed that, after peritumoral administration, both oligonucleotides accumulated mainly in the kidneys and tumor tissue (Fig. 2). The content of μ ASO and PS ASO in the kidneys after 4 h was 71% and 36% of the total amounts of the therapeutics retained in the body (Fig. 2*B*). Four hours after peritumoral administration, the relative content of oligonucleotides in the tumor was 23% for μ ASO and 63% for PS ASO. By 24 h, the excretion of μ ASO slowed, and its relative content in the tumor increased to 48% (Fig. 2*B*). The content of PS ASO in tumor tissue by 24 h decreased to 48%, with more active accumulation in the kidneys. As can be seen from the fluorescence imaging of mouse internal organs, most of the PS ASOs remained anchored in the area of administration while the μ-oligonucleotide was distributed throughout the body, providing high accumulation in the tumor tissue (Fig. 2*A*).

After i.v. administration, the main fraction of both μ and PS ASOs was localized in the kidneys and liver of animals. The content of μ and PS ASOs in the kidneys after 24 h was 90% and 77%, respectively, and 16% of PS ASO accumulated in the liver (Fig. 2 *A* and *B*). Accumulation of oligonucleotides in tumor tissue after i.v. administration was poor: By 24 h, the relative content of both oligonucleotides did not exceed 2% (Fig. 2*B*). According to the obtained data, peritumoral injections were used to study the antitumor potential of μ ASOs in vivo.

Confocal microscopy images of tumor node cryosections confirmed the accumulation of μ and PS oligonucleotides in tumor tissue (Fig. 2*C* and *SI Appendix*, Fig. S2). According to the results of confocal microscopy, both oligonucleotides localize in the intercellular space as well as in the cytoplasm and nucleus of tumor cells 24 h after injection.

Tumor Growth Retardation In Vivo by miR-21–Targeted μ and PS ASOs.
The antitumor potential of μ ASOs was studied using a xenograft KB-8-5/SCID model. The miR-21 inhibitory effect of μ ASO in KB-8-5 tumor cells was preliminarily confirmed in vitro by stem-loop PCR (*SI Appendix*, Fig. S3). At day 12, when the primary tumor node was formed, 10 μg of μ or PS ASOs in complex with cationic liposomes F were peritumorally administered to animals. In total, four injections were given at 3-d intervals (Fig. 3*A*). This treatment regimen was used based on the data on stability of the oligonucleotides in serum, kinetics of miRNA down-regulation, and biodistribution. Control groups received unloaded liposomes F or Opti-MEM culture medium.

Patutina et al.

www.manaraa.com

BIOCHEMISTRY

Fig. 2. Biodistribution of Cy5.5-labeled μ and PS ASOs in tumor-bearing SCID mice. (*A*) Lifetime fluorescence imaging of tumor-bearing SCID mice (*n* = 3 mice per group), dorsal orientation view, and dissected organs 4 and 24 h after peritumoral (pt) and i.v. (iv) injections of 40 μg per mouse of modified oligonucleotides. Control, noninjected mice. (*B*) Percent biodistribution of modified oligonucleotides after 4 and 24 h after pt and i.v. injections of μ and PS ASOs (mean ± SE). (*C*) Confocal microscopic images of cryosections of KB-8-5 tumors from mice 24 h after pt injections of Cy5.5-labeled μ and PS ASOs at a dose of 40 μg per mouse. Three-channel pictures are shown. Merged images represent staining of nucleus with DAPI (blue), staining of actin filaments with phalloidin-TRITC (green), and visualization of oligonucleotides by Cy5.5-labeling (red). Magnification ×400.

Analysis of kinetics of tumor growth revealed that PS-miR-21-ON, despite significant accumulation in tumor tissue, did not promote any statistically reliable retardation of tumor growth, and its effect was statistically insignificant in comparison with control PS-Scr-ON and unloaded liposomes F (Fig. 3*B*). In turn, μ-miR-21-ON provided an eightfold reduction of tumor volume

www.manaraa.com

Fig. 3. Antitumor effect of μ-miR-21-ON. (*A*) Experimental design including engraftment of SCID mice with human epidermoid carcinoma KB-8-5 and peritumoral injections of μ-miR-21-ON, PS-miR-21-ON, or scrambled μ or PS ASOs in complex with folate-containing liposomes F at a dose of 10 μg per mouse. In total, four injections were made at days 12, 16, 20, and 24 after tumor cell implantation. (*B*) Kinetics of KB-8-5 tumor growth after treatment with μ-miR-21-ON and PS-miR-21-ON ($n = 7$ mice per group). The days of injections are marked by arrows. An * indicates statistically significant difference of μ-miR-21-ON group from all of the other groups, with $P < 0.05$. (*C*) Doubling time of KB-8-5 tumors after treatment with oligonucleotides. Statistically reliable difference from all groups is marked by asterisk. (*D*) Tumor w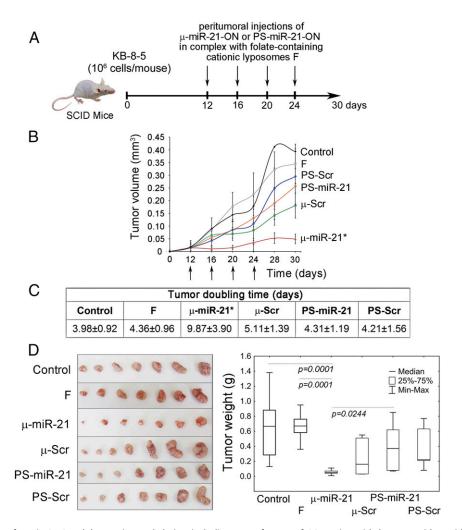eight at day 30. Data were statistically analyzed using one-way ANOVA with post hoc Tukey test; *P* value indicates a statistically reliable difference. F, liposomes F.

compared to control, fivefold compared to PS-miR-21-ON, and fourfold compared to μ-Scr-ON (Fig. 3*B*). Moreover, application of μ-miR-21-ON contributed to a considerable increase in the tumor doubling time that in average was twofold longer than in other groups (Fig. 3*C*). Comparison of tumor weights showed that the average tumor weight in the μ-miR-21-ON–injected group was up to 12-fold less than in control and about sixfold less compared to μ-Scr-ON (Fig. 3*D*). In contrast, tumor weight in groups injected with PS ASOs was only twofold less than in the control, with no reliable differences between PS-miR-21-ON and PS-Scr-ON (Fig. 3*D*).

To confirm that the antitumor effect of μ-miR-21-ON was miR-21–mediated, the levels of miR-21 and its direct protein targets PTEN and PDCD4 in tumor tissue were evaluated at the end of the experiment. μ-miR-21-ON administration caused a 50% decrease in the miR-21 level, compared to control (Fig. 4*A*), while PS-miR-21-ON administration reduced the level of miR-21 only by 25% (Fig. 4*A*). It is noteworthy that the observed effect of μ-miR-21-ON was specific: No detectable downregulation of other miRNAs, such as miR-155 and miR-17 in tumor tissue, was observed (Fig. 4*B*).

After inhibition of oncogenic miR-21, the activation of the biosynthesis of tumor suppressor proteins, among which PTEN and PDCD4 represent the most well-established targets, might be expected (20, 21). Indeed, the level of these proteins was significantly enhanced after μ-miR-21-ON treatment: 1.5-fold for PDCD4 and 3.5-fold for PTEN, compared to control, while μ-Scr-ON, PS-miR-21-ON, and PS-Scr-ON had no detectable impact on the expression of these proteins (Fig. 4 *C* and *D*).

Histological Analysis of KB-8-5 Tumors after Treatment with miR-21–Targeted μ and PS ASOs. Microscopic examination of KB-8-5 carcinomas showed that tumor tissue is represented by polymorphic epidermal cancer cells with acidophilic cytoplasm, a large nucleus with two to three hyperchromic nucleoli, and a high mitotic rate (Fig. 5). Necrotic changes and inflammatory infiltration, represented predominantly by lymphocytes with a small number of neutrophils and macrophages located at the border of unaltered tumor tissue and necrosis, were found in the tumors of all groups (*SI Appendix*, Table S1). However, in the group treated by μ-miR-21-ON, areas of necrosis and inflammation were much smaller than in other groups (*SI Appendix*, Table S1).
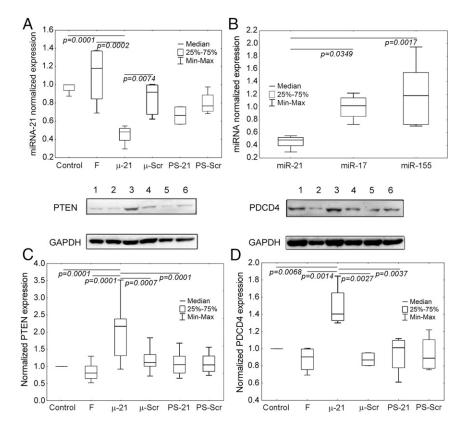
BIOCHEMISTRY

www.manaraa.com

Fig. 4. The level of miRNAs and proteins PTEN and PDCD4 in human epidermoid carcinoma KB-8-5 tissue after administration of μ-miR-21-ON and PS-miR-21-ON. (*A*) The level of miR-21 in tumor tissue after completion of treatment with μ-miR-21-ON and PS-miR-21-ON. (*B*) The level of miR-21, miR-155, and miR-17 after treatment with μ-miR-21-ON. Expression of miRNAs was measured by qPCR and normalized to the expression of snRNA U6. (*C* and *D*) Expression of tumor suppressor proteins PTEN and PDCD4, respectively, after treatment with μ-miR-21-ON and PS-miR-21-ON measured by Western blot. Protein levels were normalized to the level of GAPDH. Numbers indicate the following groups: 1, control; 2, folate-containing liposomes F; 3, μ-miR-21-ON; 4, μ-Scr-ON; 5, PS-miR-21-ON; 6, Ps-Scr-ON. Data were statistically analyzed using one-way ANOVA with post hoc Tukey test; *P* value indicates a statistically reliable difference.

The smaller size of the primary tumor node in this group and its trophic and blood supply may have significant influence on these parameters.

Histological analysis showed that tumor tissue of μ-miR-21-ON–treated mice was characterized by fourfold reduced mitotic activity, as compared to the control group, and twofold reduced, as compared to groups treated with μ-Scr-ON and PS-miR-21-ON (Fig. 5 *A* and *B*). Morphometric analysis of caspase-3 immunohistochemical images demonstrated that nontreated KB-8-5 tumor tissue had a small number of apoptotic cells (Fig. 5 *C* and *D*). μ-miR-21-ON treatment led to a 12.8-fold increase in the number of caspase-3 positive cells as compared with the control group (*P* = 0.0001) (Fig. 5*D*). Administration of oligonucleotides, regardless of target specificity and modification type, led to an increase in the number of apoptotic cells in tumor tissue, but the average number of apoptotic cells in the μ-miR-21-ON–treated group was 1.5-fold higher compared to groups of mice injected with other oligonucleotides. However, due to the increase in the scatter of experimental data, statistically significant differences between the number of caspase-3 positive cells were observed only after the treatment with μ-miR-21-ON and PS-Scr (*P* = 0.0005) (Fig. 5*D*).

Toxicity of Oligonucleotides. Biochemical blood tests showed that μ ASOs exhibited no toxic effect on the liver and kidneys of mice. No statistically significant differences in blood indicators, such as ALT, ALK, total protein, creatinine, and blood urea nitrogen (BUN), between the groups (including healthy mice) were found (*SI Appendix*, Table S2).

The development of a KB-8-5 tumor, per se, has a distinguishable toxic effect on the liver, manifested in an increase in destructive changes (dystrophy plus necrosis) up to 35% from the entire liver parenchyma (*SI Appendix*, Fig. S4 and Table S3). Administration of ASOs caused no additional detrimental effect on the liver. Moreover, in the groups treated with μ-miR-21-ON or PS-miR-21-ON, a significantly reduced percentage of destructive changes in the liver parenchyma was observed, which reflects a therapeutic effect. Tumor development as well as applied therapy did not affect the regenerative properties of the liver: No changes in numerical density of binuclear hepatocytes were observed (*SI Appendix*, Table S3).

Morphometric analysis of kidneys showed that, upon tumor development, the normal kidney tissue reduced to about 75% (*SI Appendix*, Table S4). In the group treated with PS ASOs, some increase in destructive changes in the kidney tissue was observed: 25 to 27% (compared to 23 to 24% in other experimental groups), manifested in dystrophy of the epithelium of the proximal tubules (*SI Appendix*, Fig. S4 and Table S4). Despite the predominant localization of both μ and PS ASOs in the kidney, signs of dystrophy were most pronounced only in the groups injected with PS ASOs.

Discussion

Over the history of the development of nucleic acid therapeutics, more than two dozen modifications of internucleotidic bonds in
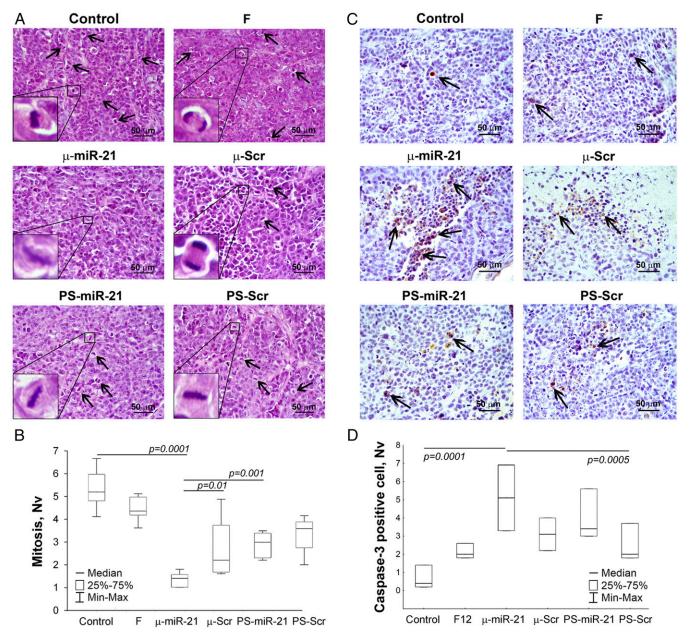
Patutina et al.

www.manaraa.com

Fig. 5. Mitosis and apoptosis in KB-8-5 tumors after therapy with μ-miR-21-ON and PS-miR-21-ON. (*A*) Typical images of tumor sections after hematoxylin and eosin staining. Magnification ×400. Bar corresponds to 50 μm. Mitoses are indicated by arrows. Typical examples of individual mitotic events are shown with magnification ×1,000 in the bottom left corner. (*B*) Morphometric analysis of tumor tissue with mitosis counting. (*C*) Typical images of tumor sections after immunohistochemical staining with caspase-3 monoclonal antibodies. Examples of caspase-3–positive cells are indicated by arrows. Magnification ×400. (*D*) Morphometric analysis of tumor tissue with apoptotic cells counting. Nv ×400. Nv, the numerical density indicating the number of particles in the unit tissue volume. Data were statistically analyzed using one-way ANOVA with post hoc Tukey test; *P* value indicates a statistically reliable difference.

oligonucleotides have been proposed, in which the phosphodiester backbone was replaced by different variants of phosphorothioates, methylphosphonates, phosphoramidates, phosphotriesters, phosphorodithioates, or derivatives with guanidinium groups or *S*-methylthiourea motifs (22–24). Among the proposed modifications, the most successful are phosphorothioates. Although this chemical substitution is endued with a number of beneficial properties, the presence of serious shortcomings (4, 5, 25–27) has led to a search for new, improved modifications. In this regard, the μ-modification has a number of important favorable properties, including exceptional resistance to nucleases, high affinity for the RNA targets, and faster RNA degradation by RNase H, compared

to PS ASOs (12). The listed biological characteristics of μ ASOs are directly reflected in the duration of functioning within the cell and the strength of silencing effect. The visible effect of μ ASOs lasts for at least 6 d, achieving 80 to 95% down-regulation of miRNA level, while PS ASOs caused only a twofold decrease, and it expired after 1 d. The main in vitro and in vivo characteristics of μ-oligonucleotides in comparison with phosphorothioate analogs are summarized in Table 1.

An important difference between μ and PS ASO is the ability of phosphorothioates to penetrate inside the cells in a carrier-free mode (28, 29). In the study of antitumor activity of μ-miR-21-ON in vivo, both oligomers were enclosed in folate-containing

BIOCHEMISTRY

www.manaraa.com

lipoplexes in order to equalize the conditions of their delivery to tumor cells. The biodistribution data showed that μ ASO rapidly spread throughout the body, ensuring efficient accumulation in tumors, while phosphorothioate oligonucleotides are characterized by anchoring in the area of administration and lower penetration efficiency into the tumor tissue. At 24 h postinjection, both μ and PS ASOs were almost equally distributed between tumor and kidney (Fig. 2).

The study of antitumor potential showed that μ-miR-21-ON provides drastic retardation of tumor growth, up to 90% 3 d after the first injection, which lasted up to 30 d until the end of the experiment. The antitumor effect of μ-miR-21-ON was accompanied by a significant decrease in mitotic activity and stimulation of proapoptotic, but not necrotic, behavior of tumor cells. μ-miR-21-ON administered to mice specifically decreased the miR-21 level in tumor observed even a week after the last injection; that was not the case for PS-miR-21-ON therapy. Moreover, during this period, a μ-miR-21-ON–mediated increase in expression of tumor suppressor proteins such, as PTEN and PDCD4, was maintained. These data demonstrate the specific and potent therapeutic effect of μ-miR-21-ON whereas the effect of PS-miR-21-ON is not so pronounced and unspecific. Earlier, it was noticed that efficient uptake of PS ASOs by cells does not always result in a pharmacologically functional intracellular pathway and therapeutic activity (30, 31).

According to the results of in vivo experiments, it seems that μ-Scr-ON is exerting some effects on tumor cells. The obtained data show that administration of oligonucleotides of any type, regardless of target specificity, leads to a moderate nontargeted effect and an increase in the scatter of experimental parameters within the group. It should be emphasized that there were no statistically significant differences between the effects of μ-Scr-ON and PS-Scr-ON, as well as PS-miR-21-ON. Moreover, our experiments have shown that no decrease in the level of miR-21, miR-17, or miR-155 was detected in response to μ-Scr-ON, thus additionally indicating the nontargeted systemic response to oligonucleotide administration. It cannot be excluded that this nontargeted effect can be not only of negative nature, resulting from general cytotoxicity, but also has a positive character,

providing an immunomodulatory or immunostimulating effect, leading to tumor regression.

The use of targeted folate-equipped cationic liposomes allowed one not only to balance the delivery of μ and PS ASOs into the tumor, but also to reduce the dose of the administered compounds, as well as mitigate their possible toxicity. For instance, in vivo administration of PS ASOs in a carrier-free mode requires doses of 20 mg/kg for the inhibition of tumor growth (32). Application of targeted delivery systems provides the decrease in PS ASO dose to 2 mg/kg (10 μg per mice), which is sufficient for their effective accumulation in tumor tissue (33). The study of blood biochemistry showed that neither the presence of a tumor, nor the therapy performed, has an effect on the level of liver and kidney enzymes. Moreover, it has been shown that the effect of both μ- and PS ASOs on the tumor process apparently reduces the total destructive changes in the liver tissue.

The other side of the ability of phosphorothioates to circulate in the body for a long time is the off-target effects associated with nonspecific interactions. The use of μ-oligonucleotides with higher therapeutic performance formulated in cationic liposomes or other nanoparticles or conjugated to some chemical moieties that interact with cell-specific receptors for effective tissue delivery seems to be safer and advantageous. In this direction, the use of N-acetylgalactosamine (GalNAc) moiety, providing interaction with asialoglycoprotein receptors, conjugated to antisense oligonucleotide was shown to greatly expand the therapeutic opportunities of ASOs (34–36). Conjugation of the GalNAc ligand to gapmer PS ASOs attenuates toxicity and promotes penetration into cells by a productive endocytic pathway that leads to a 30-fold increase in therapeutic potency and at least a 40-fold decrease in the dosage of PS ASOs (35, 37).

The high performance of antisense therapy in vivo is determined to a large extent by the appropriate RNA target choice. Selected in the study, miR-21 represents a crucial regulator of a plethora of cellular processes, such as proliferation, differentiation, apoptosis, migration, etc. (38–41). As a result, inhibition of the aberrant hyperactivity of miR-21 in tumor tissue leads to global changes in cellular signaling pathways and promotes

Table 1. Comparison of biological properties of μ and PS ASOs

Biological properties	Mesyl phosphoramidate (μ) ASO	Phosphorothioate (PS) ASO
In vitro (12)		
Hybridization efficiency in equimolar concentration with miRNA, %	100	46
Stability in 10% fetal bovine serum, $t_{1/2}$, h	>168	96
RNase H cleavage rate, $k\ obs$, $10^{-6} \cdot s^{-1}$	28.3 ± 2.2	8.7 ± 0.6
Efficiency of miRNA down-regulation in tumor cells, 72 h, %	75 to 90	—**
Duration of miRNA down-regulation in tumor cells, h	>144	<72
Inhibition of tumor cell migration, 72 h	19-fold	Fivefold
In vivo		
Reduction in tumor growth*		
Average tumor volume	Eightfold	Twofold
Average tumor weight	12-fold	Twofold
Tumor doubling time, d	9.9 ± 2.9	4.3 ± 1.2
Decrease in mitosis	3.9-fold	1.8-fold
Increase in caspase-3 positive cells	12.8-fold	8.5-fold
Efficiency of miRNA down-regulation in tumor tissue, %*	50	25
Increase in tumor suppressor protein expression in tumor tissue, fold*	1.5- to 3.5-fold	—**
Toxicity		
Blood biochemistry	No	No
Liver	No	No
Kidney	No	Moderate

*The effect was measured 7 d after the last administration of ASO.
**No effect was observed.

www.manaraa.com

manifold reinforcement of tumor suppressor protein synthesis, such as PTEN, PDCD4, RhoB, LATS1, MGMT, and TP53, exerting potent antitumor action on several carcinogenesis processes simultaneously (42, 43).

In conclusion, the designed oligonucleotides are worth attention as they are new highly effective uniformly modified DNA analogs that do not require additional modifications and substitutions, which synthesis is easily acceptable in a solid-phase platform. The biological antitumor potential of μ ASOs targeted to highly oncogenic miR-21 is successfully realized in vivo, leading to a drastic retardation of tumor growth in mice, contributing to the effective and specific inhibition of key carcinogenesis processes—reduction of tumor cell mitotic activity and induction of apoptotic cell death. Thus, mesyl phosphoramidate oligonucleotides are a novel potent tool of antisense technology and, in certain cases, an attractive alternative to phosphorothioate ASOs.

Materials and Methods

Oligonucleotides. μ-oligonucleotides were assembled by automated solid-phase synthesis from commercial 5′-dimethoxytrityl (DMTr) β-cyanoethyl N,N-diisopropyl 3′-phosphoramidites and controlled pore glass supports by substituting a Staudinger reaction with methanesulfonyl azide (0.5 M in acetonitrile, 30 min at ambient temperature) for aqueous iodine oxidation in each cycle of nucleotide incorporation, as described previously (11). After the completion of the synthesis, oligonucleotides were cleaved from the polymer support and deprotected by standard ammonia treatment. PS oligodeoxynucleotides were prepared by sulfurization with Sulfurizing Reagent II [3-((dimethylaminomethyliden)amino)-3H-1,2,4-dithiazol-3-thione] (Glen Research) following the manufacturer's protocol. Analysis and purification of μ-oligonucleotides were performed by electrophoresis in 20% denaturing polyacrylamide gel electrophoresis (PAGE). The bands in the gels were visualized by ultraviolet (UV) shadowing and excised, and oligonucleotides were eluted with 0.3 M NaClO$_4$, desalted on a NAP-25 column by elution with deionized water, and freeze-dried. To obtain Cy5.5-labeled oligonucleotides, the respective 3′-aminoalkyl mesyl phosphoramidate and phosphorothioate oligonucleotides assembled on 3′-Amino-modifier C7 CPG (Glen Research) were acylated with Cy5.5 N-hydroxysuccinimide ester (Lumiprobe) and purified as described above.

The following oligonucleotides were prepared for the study (symbols μ and S designate mesyl phosphoramidate and phosphorothioate internucleotidic groups, respectively): μ-miR-21-ON 5′-TᴹCᴹAᴹAᴹCᴹAᴹTᴹCᴹAᴹGᴹTᴹCᴹTᴹGᴹAᴹTᴹAᴹAᴹGᴹCᴹTᴹA; Cy5.5-μ-miR-21-ON 5′-TᴹCᴹAᴹAᴹCᴹAᴹTᴹCᴹAᴹGᴹTᴹCᴹTᴹGᴹAᴹTᴹAᴹAᴹGᴹCᴹTᴹA-Cy5.5; μ-miR-155-ON 5′-AᴹiᴹCᴹCᴹCᴹCᴹTᴹAᴹTᴹCᴹAᴹCᴹGᴹAᴹTᴹTᴹAᴹGᴹCᴹAᴹTᴹTᴹAᴹA; μ-miR-17-ON 5′-CᴹTᴹAᴹCᴹCᴹTᴹGᴹCᴹAᴹCᴹTᴹGᴹTᴹAᴹAᴹGᴹCᴹAᴹCᴹTᴹTᴹTᴹG; μ-Scr-ON 5′-CᴹAᴹAᴹGᴹTᴹCᴹTᴹCᴹGᴹTᴹAᴹTᴹGᴹTᴹAᴹGᴹTᴹGᴹGᴹTᴹT; PS-miR21-ON 5′-T$_S$C$_S$A$_S$A$_S$C$_S$A$_S$T$_S$C$_S$A$_S$G$_S$T$_S$C$_S$T$_S$G$_S$A$_S$T$_S$A$_S$A$_S$G$_S$C$_S$T$_S$A; Cy5.5-PS-miR-21-ON 5′-T$_S$C$_S$A$_S$A$_S$C$_S$A$_S$T$_S$C$_S$A$_S$G$_S$T$_S$C$_S$T$_S$G$_S$A$_S$T$_S$A$_S$A$_S$G$_S$C$_S$T$_S$A-Cy5.5; and PS-Scr-ON 5′-C$_S$A$_S$A$_S$G$_S$T$_S$C$_S$T$_S$C$_S$G$_S$T$_S$A$_S$T$_S$G$_S$T$_S$A$_S$G$_S$T$_S$G$_S$G$_S$T$_S$T.

Transfection of Tumor Cells with ASOs. Transfection of mouse B16 melanoma cells (obtained from the Cell Culture Bank of the Blokhin National Medical Oncology Research Center, Moscow, Russia) was performed by using Lipofectamine 2000 (Invitrogen) according to the manufacturer's protocol as described previously (12). The cells were incubated at 37 °C in a humidified atmosphere with 5% CO$_2$ for 4 h. The medium then was replaced with Dulbecco's modified Eagle's medium (DMEM) containing 10% fetal bovine serum (FBS) and 1% antibiotic antimycotic solution (10,000 μg/mL streptomycin, 10,000 IU/mL penicillin, and 25 μg/mL amphotericin), and the cells were further cultivated for 144 h.

Preparation of the Complexes of Cationic Liposomes and Oligonucleotides. Prior to use in in vivo studies, the cationic folate-containing liposomes F (19) and modified oligonucleotide were mixed to form lipoplexes in a serum-free Opti-MEM by vigorous mixing of equal volumes of liposomes and respective ASO solutions in Opti-MEM taken at 100 μg/mL concentration. Lipoplexes were prepared at an N/P ratio of 4/1, where N/P is a ratio between nitrogen atoms of polycationic lipid and lipid helper in liposomes and phosphorus atoms of oligonucleotides. The resulting mixtures were incubated for 20 min at room temperature and used for in vivo treatment.

Mice. Male 10- to 12-wk-old SCID mice were kept with a natural light regime on a standard diet for laboratory animals (State Standard [GOST] R 5025892) in compliance with the international recommendations of the European Convention for the Protection of Vertebrate Animals Used for Experimental

Studies (1997), as well as the rules of laboratory practice in the performance of preclinical studies in the Russian State Standards (R 51000.3-96 and 51000.4-96). The experimental protocol (no. 53) was approved by the Committee on the Ethics of Animal Experiments with the Institute of Cytology and Genetics Siberian Branch of the Russian Academy of Sciences (SB RAS).

In Vivo Biodistribution Studies. In vivo real-time fluorescence imaging was used to evaluate the distribution of Cy5.5-labeled μ-miR-21-ON and PS-miR-21-ON in KB-8-5 tumor-bearing SCID mice. The in vivo MS FX PRO Imaging System (Carestream) was used to obtain X-rays and, concurrently, near-infrared fluorescence (NIRF) images (Cy5.5: excitation 620 nm, emission 700 nm). Mice (n = 3 per each group) were injected i.v. (200 μL) or peritumorally (100 μL) with 40 μg per mouse of Cy5.5-labeled μ-miR-21-ON or PS-miR-21-ON precomplexed with liposomes F. Animals were anesthetized with isoflurane and placed on a heating tray (37 °C). The fluorescence (10-s exposure) and X-ray (15-s exposure) scans were performed at 4 and 24 h postinjection. At the end of the experiment, mice were killed, and lungs, heart, liver, spleen, kidneys, and tumor were collected, and the fluorescence intensity of each organ was detected. Two parameters reflecting the efficiency of Cy5.5-labeled oligonucleotide accumulation in the organs were used for comparison: organ fluorescence intensity, measured in relative fluorescent units (RFUs), and the percentage of organ fluorescence intensity relative to the total fluorescent intensity of all organs. Images were batch exported as 16-bit tag image file format (tiffs), and overlays were completed in Adobe Photoshop CS3 (v 10.0).

Confocal Microscopy. After imaging, tumors were immediately mixed with Tissue-Tek O.C.T. (Sakura) and frozen in liquid nitrogen. The samples were kept at −70 °C until processing. Sections 7 μm thick were cut in a Microm HM 505N cryostat (Microm) at −21 °C. The cryosections of tumor tissues were stained with DAPI and phalloidin-tetramethylrhodamine B isothiocyanate (TRITC) according to the standard protocol and mounted in ProLong Gold Antifade Mountant (Life Technologies). Finally, the cryosections were observed using an LSM 780 confocal fluorescent microscope (Carl Zeiss) at 20× magnification using band-pass (BP) 420- to 480-nm, BP 505- to 530-nm, and long-pass (LP) 560-nm optical filters. Microscopic analysis was carried out at the Multiple-Access Center for Microscopy of Biological Subjects (Institute of Cytology and Genetics SB RAS, Novosibirsk, Russia).

Antitumor Studies In Vivo. Human epidermoid carcinoma KB-8-5 tumors were initiated in SCID mice by subcutaneous (s.c.) injection of KB-8-5 cells (generously provided by M. Gottesman, NIH, Bethesda, MD), 10^6 in 0.1 mL in sterile saline buffer, into the left flank. At day 12 after transplantation, when tumors began to be palpable, mice were divided into six groups according to further treatment (n = 7 mice per group): 1) control (Opti-MEM); 2) F (unloaded folate-containing liposomes F); 3) μ-miR-21-ON; 4) μ-Scr-ON; 5) PS-miR-21-ON, and 6) PS-Scr-ON. Oligonucleotides precomplexed with liposomes F at an N/P ratio of 4/1 were peritumorally injected at a concentration of 10 μg per mice every 4 d. Four injections were made in total. The dose was calculated according to the data on efficiency of nucleic acid delivery using folate-containing liposomes (19) to ensure an intratumoral concentration of at least 100 nM, which provides an efficient decrease in miR-21 level (12) (see also *SI Appendix*, Fig. S1). The tumor volumes were measured every 3 d using calipers in investigator-blinded fashion. Tumor volumes were calculated as V = (π/6 × length × width × height). At day 30, animals were killed, and tumors and internal organs, including livers and kidneys, were collected and fixed in 10% neutral-buffered formalin (BioVitrum) for further histological analysis. A quarter of each tumor node was collected to isolate total RNA and to prepare lysates for Western blot analysis. Tumor doubling time (DT) was estimated as follows: DT = (t − t$_0$) × ln 2/(ln V − ln V$_0$) where (t − t$_0$) indicates the length of time between two measurements of tumor size, and V$_0$ and V denote the tumor volume at two points of the measurement (44).

qPCR. After treatment with oligonucleotides, total RNA was isolated using TRIzol Reagent (Invitrogen) according to the manufacturer's protocol. After in vitro transfection of mouse B16 melanoma cells, total RNA was extracted from tumor cells at time points 24, 48, 72, 96, and 144 h. After in vivo therapy, RNA from human epidermoid carcinoma KB-8-5 tumor tissue was isolated at day 30 by homogenization of tumor samples in TRIzol. The level of miRNAs in B16 cells or KB-8-5 tumors was measured using stem-loop qPCR technology (45, 46). Complementary DNA (cDNA) synthesis was carried out using SuperScript III reverse transcriptase (SSIII RT; Invitrogen) as previously described (47, 48). The RT and PCR primers used in the study are listed in *SI*

www.manaraa.com

Appendix, Table S5. PCR amplification was carried out using BioMaster HS-qPCR SYBR Blue mix (Biolabmix) according to the manufacturer's protocol. The obtained qPCR data were analyzed by standard Bio-Rad iQ5 v.2.0 software. For each sample, the threshold cycle (Ct) was determined. Quantitative assessment of the level of transcript representation and relative miRNA expression was performed by comparing the Ct values for miRNA and U6 small nuclear RNA (snRNA) used as a reference.

Western Blot Analysis. To prepare cell lysates from KB-8-5 tumors, tumor tissue specimens were homogenized in radioimmunoprecipitation assay (RIPA) buffer (Thermo Scientific) using an electric homogenizer, followed by centrifugation at +4 °C (12,000 rpm, 20 min). Collected cell lysates were separated in 12.5% sodium dodecyl sulfate (SDS)/PAGE and transferred to a poly(vinylidene difluoride) (PVDF) membrane using a semidry transfer. Western Blot analysis was performed as described earlier (47, 48) using primary antibodies against PTEN (ab154812, 1:800; Abcam), PDCD4 (ab79405, 1:1,000; Abcam), and GAPDH (ab9485, 1:2,000; Abcam), and secondary HRP-conjugated goat anti-rabbit antibodies (ab6721; Abcam).

Histology. Histological analysis was performed similar to ref. 49. Briefly, the specimens of fixed tumors, kidneys, and livers from each animal were dehydrated in ascending ethanols and xylols and embedded in HISTOMIX paraffin (BioVitrum). Paraffin sections (5 μm) were sliced on a Microm HM 355S microtome (Thermo Fisher Scientific) and stained with hematoxylin and eosin, microscopically examined, and scanned. Tumor sections for immunohistochemical (IHC) studies (3 to 4 μm) were deparaffinated and rehydrated; antigen retrieval was carried out after exposure in a microwave oven at 700 W. The samples were incubated with the caspase-3 (ab2302, Abcam) specific antibodies according to the manufacturer's protocol. Next, the sections were incubated with secondary HRP-conjugated antibodies (Spring Bioscience detection system), exposed to 3,3'-diaminobenzidine (DAB) substrate, and stained with Mayer's hematoxylin. Images were obtained using an Axiostar Plus microscope equipped with an Axiocam MRc5 digital camera (Zeiss) at 100× and 400× magnifications. Twenty random fields were studied in each specimen, comprising 140 fields for each group of mice.

Morphometric analysis of tumor, liver, and kidney sections was performed as described in ref. 49 by point counting, using a counting grid which consists of 100 testing points in a testing area equal to 3.2×10^6 μm^2. Ten to 15 random fields were studied in each specimen, comprising 70 to 100 fields for each group of mice in total during morphometric analyses of liver and kidney, and 20 to 50 random fields were studied in each specimen, comprising 140 to 350 fields for each group of mice in total during morphometric analyses of tumors. Morphometric analysis of tumor tissue included evaluation of the volume densities (Vv, %) of unaltered tumor tissue, lymphoid infiltration, necrosis, total destructive changes (lymphoid infiltration plus necrosis), and numerical density (Nv) of mitoses and caspase-3–positive cells in tumor tissue. The ratio of unaltered tumor tissue to mutilated tumor tissue was estimated.

The volume density (Vv, %) representing the volume fraction of tissue occupied by this compartment was determined from the points lying over this structure and calculated using the following formula: Vv = (Pstructure/Ptest) × 100%, where Pstructure denotes the number of points over the structure and Ptest denotes the total number of test points, in this case 100. The numerical density (Nv) indicating the number of particles in the unit tissue volume was evaluated as the number of particles in the square unit, 3.2×10^6 μm^2 in this case.

Statistics. The data obtained were statistically processed using one-way ANOVA and post hoc Tukey test ($P \leq 0.05$). The statistics package STATISTICA version 10.0 was used for this analysis.

Data Availability. All study data are included in the article and *SI Appendix*.

1. S. T. Crooke, J. L. Witztum, C. F. Bennett, B. F. Baker, RNA-targeted therapeutics. *Cell Metab.* 27, 714–739 (2018).
2. X. Shen, D. R. Corey, Chemistry, mechanism and clinical status of antisense oligonucleotides and duplex RNAs. *Nucleic Acids Res.* 46, 1584–1600 (2018).
3. F. Eckstein, Phosphorothioates, essential components of therapeutic oligonucleotides. *Nucleic Acid Ther.* 24, 374–387 (2014).
4. W. Shen et al., Chemical modification of PS-ASO therapeutics reduces cellular protein-binding and improves the therapeutic index. *Nat. Biotechnol.* 37, 640–650 (2019).
5. M. T. Migawa et al., Site-specific replacement of phosphorothioate with alkyl phosphonate linkages enhances the therapeutic profile of gapmer ASOs by modulating interactions with cellular proteins. *Nucleic Acids Res.* 47, 5465–5479 (2019).
6. P. J. Kamola et al., Strategies for in vivo screening and mitigation of hepatotoxicity associated with antisense drugs. *Mol. Ther. Nucleic Acids* 8, 383–394 (2017).
7. S. Kakiuchi-Kiyota et al., Comparison of hepatic transcription profiles of locked ribonucleic acid antisense oligonucleotides: Evidence of distinct pathways contributing to non-target mediated toxicity in mice. *Toxicol. Sci.* 138, 234–248 (2014).
8. P. J. Kamola et al., *In silico* and *in vitro* evaluation of exonic and intronic off-target effects form a critical element of therapeutic ASO gapmer optimization. *Nucleic Acids Res.* 43, 8638–8650 (2015).
9. D. Heindl, D. Kessler, A. Schube, W. Thuer, A. Giraut, Easy method for the synthesis of labeled oligonucleotides. *Nucleic Acids Symp. Ser. (Oxf.)* 52, 405–406 (2008).
10. D. V. Prokhorova, B. P. Chelobanov, E. A. Burakova, A. A. Fokina, D. A. Stetsenko, New oligodeoxyribonucleotide derivatives bearing internucleotide N-tosyl phosphoramidate groups: Synthesis and complementary binding to DNA and RNA. *Russ. J. Bioorganic Chem.* 43, 38–42 (2017).
11. B. P. Chelobanov, E. A. Burakova, D. V. Prokhorova, A. A. Fokina, D. A. Stetsenko, New oligodeoxynucleotide derivatives containing N-(methanesulfonyl)-phosphoramidate (mesyl phosphoramidate) internucleotide group. *Russ. J. Bioorganic Chem.* 43, 664–668 (2017).
12. S. K. Miroshnichenko et al., Mesyl phosphoramidate antisense oligonucleotides as an alternative to phosphorothioates with improved biochemical and biological properties. *Proc. Natl. Acad. Sci. U.S.A.* 116, 1229–1234 (2019).
13. L. E. B. Buscaglia, Y. Li, Apoptosis and the target genes of microRNA-21. *Chin. J. Cancer* 30, 371–380 (2011).
14. S. Li, Z. Liang, L. Xu, F. Zou, MicroRNA-21: A ubiquitously expressed pro-survival factor in cancer and other diseases. *Mol. Cell. Biochem.* 360, 147–158 (2012).
15. S. R. Pfeffer, C. H. Yang, L. M. Pfeffer, The role of miR-21 in cancer. *Drug Dev. Res.* 76, 270–277 (2015).
16. D. Sekar, P. Mani, M. Biruntha, P. Sivagurunathan, M. Karthigeyan, Dissecting the functional role of microRNA 21 in osteosarcoma. *Cancer Gene Ther.* 26, 179–182 (2019).
17. W. Zheng et al., MicroRNA-21: A promising biomarker for the prognosis and diagnosis of non-small cell lung cancer. (Review). *Oncol. Lett.* 16, 2777–2782 (2018).
18. M. Correia de Sousa, M. Gjorgjieva, D. Dolicka, C. Sobolewski, M. Foti, Deciphering miRNAs' action through miRNA editing. *Int. J. Mol. Sci.* 20, 6249 (2019).
19. T. O. Kabilova et al., Targeted delivery of nucleic acids into xenograft tumors mediated by novel folate-equipped liposomes. *Eur. J. Pharm. Biopharm.* 123, 59–70 (2018).
20. H. Fang et al., miRNA-21 promotes proliferation and invasion of triple-negative breast cancer cells through targeting PTEN. *Am. J. Transl. Res.* 9, 953–961 (2017).
21. Z. Wang et al., Reduction of miR-21 induces SK-N-SH cell apoptosis and inhibits proliferation *via* PTEN/PDCD4. *Oncol. Lett.* 13, 4727–4733 (2017).
22. A. De Mesmaeker, K. H. Altmann, A. Waldner, S. Wendeborn, Backbone modifications in oligonucleotides and peptide nucleic acid systems. *Curr. Opin. Struct. Biol.* 5, 343–355 (1995).
23. M. Meng, C. Ducho, Oligonucleotide analogues with cationic backbone linkages. *Beilstein J. Org. Chem.* 14, 1293–1308 (2018).
24. H. Šipova et al., 5'-O-Methylphosphonate nucleic acids—New modified DNAs that increase the Escherichia coli RNase H cleavage rate of hybrid duplexes. *Nucleic Acids Res.* 42, 5378–5389 (2014).
25. K. Hovingh, J. Besseling, J. Kastelein, Efficacy and safety of mipomersen sodium (Kynamro). *Expert Opin. Drug Saf.* 12, 569–579 (2013).
26. S. P. Henry, H. Bolte, C. Auletta, D. J. Kornbrust, Evaluation of the toxicity of ISIS 2302, a phosphorothioate oligonucleotide, in a four-week study in cynomolgus monkeys. *Toxicology* 120, 145–155 (1997).
27. E. E. Swayze et al., Antisense oligonucleotides containing locked nucleic acid improve potency but cause significant hepatotoxicity in animals. *Nucleic Acids Res.* 35, 687–700 (2007).
28. S. T. Crooke, S. Wang, T. A. Vickers, W. Shen, X. H. Liang, Cellular uptake and trafficking of antisense oligonucleotides. *Nat. Biotechnol.* 35, 230–237 (2017).
29. R. L. Juliano, K. Carver, Cellular uptake and intracellular trafficking of oligonucleotides. *Adv. Drug Deliv. Rev.* 87, 35–45 (2015).
30. R. S. Geary, D. Norris, R. Yu, C. F. Bennett, Pharmacokinetics, biodistribution and cell uptake of antisense oligonucleotides. *Adv. Drug Deliv. Rev.* 87, 46–51 (2015).
31. E. Koller et al., Mechanisms of single-stranded phosphorothioate modified antisense oligonucleotide accumulation in hepatocytes. *Nucleic Acids Res.* 39, 4795–4807 (2011).
32. K. Seystahl et al., Biological role and therapeutic targeting of TGF-b3 in glioblastoma. *Mol. Cancer Ther.* 16, 1177–1186 (2017).
33. Y. Ma et al., Structural optimization and additional targets identification of antisense oligonucleotide G3139 encapsulated in a neutral cytidinyl-lipid combined with a cationic lipid in vitro and in vivo. *Biomaterials* 197, 182–193 (2019).
34. J. K. Nair et al., Multivalent N-acetylgalactosamine-conjugated siRNA localizes in hepatocytes and elicits robust RNAi-mediated gene silencing. *J. Am. Chem. Soc.* 136, 16958–16961 (2014).
35. T. P. Prakash et al., Targeted delivery of antisense oligonucleotides to hepatocytes using triantennary N-acetyl galactosamine improves potency 10-fold in mice. *Nucleic Acids Res.* 42, 8796–8807 (2014).

Patutina et al.

www.manaraa.com

36. R. Z. Yu *et al*., Disposition and pharmacology of a GalNAc3-conjugated ASO targeting human lipoprotein (a) in mice. *Mol. Ther. Nucleic Acids* **5**, e317 (2016).

37. S. Sewing *et al*., GalNAc conjugation attenuates the cytotoxicity of antisense oligonucleotide drugs in renal tubular cells. *Mol. Ther. Nucleic Acids* **14**, 67–79 (2019).

38. B. Zhou *et al*., Effect of miR-21 on apoptosis in lung cancer cell through inhibiting the PI3K/Akt/NF-κB signaling pathway in vitro and in vivo. *Cell. Physiol. Biochem.* **46**, 999–1008 (2018).

39. M. Koutsioumpa *et al*., MKAD-21 suppresses the oncogenic activity of the miR-21/ PPP2R2A/ERK molecular network in bladder cancer. *Mol. Cancer Ther.* **17**, 1430–1440 (2018).

40. W. J. Wang *et al*., MiR-21 promotes ECM degradation through inhibiting autophagy *via* the PTEN/akt/mTOR signaling pathway in human degenerated NP cells. *Biomed. Pharmacother.* **99**, 725–734 (2018).

41. Y. Su *et al*., The IGF-I/JAK2-STAT3/miR-21 signaling pathway may be associated with human renal cell carcinoma cell growth. *Cancer Biomark.* **19**, 289–296 (2017).

42. F. An, Y. Liu, Y. Hu, miR-21 inhibition of LATS1 promotes proliferation and metastasis of renal cancer cells and tumor stem cell phenotype. *Oncol. Lett.* **14**, 4684–4688 (2017).

43. J. Carabia *et al*., Microenvironment regulates the expression of miR-21 and tumor suppressor genes PTEN, PIAS3 and PDCD4 through ZAP-70 in chronic lymphocytic leukemia. *Sci. Rep.* **7**, 12262 (2017).

44. S. Ozono *et al*.; Japanese Society of Renal Cancer, Tumor doubling time of renal cell carcinoma measured by CT: Collaboration of Japanese society of renal cancer. *Jpn. J. Clin. Oncol.* **34**, 82–85 (2004).

45. C. Chen *et al*., Real-time quantification of microRNAs by stem-loop RT-PCR. *Nucleic Acids Res.* **33**, e179 (2005).

46. E. Varkonyi-Gasic, R. P. Hellens, Quantitative stem-loop RT-PCR for detection of microRNAs. *Methods Mol. Biol.* **744**, 145–157 (2011).

47. O. A. Patutina *et al*., miRNases: Novel peptide-oligonucleotide bioconjugates that silence miR-21 in lymphosarcoma cells. *Biomaterials* **122**, 163–178 (2017).

48. O. A. Patutina *et al*., Peptide-oligonucleotide conjugates exhibiting pyrimidine-X cleavage specificity efficiently silence miRNA target acting synergistically with RNase H. *Sci. Rep.* **8**, 14990 (2018).

49. E. P. Goncharova *et al*., Immunostimulating RNA delivered by p1500 PEGylated cationic liposomes limits influenza infection in c57Bl/6 mice. *Pharmaceutics* **12**, 875 (2020).

BIOCHEMISTRY

Patutina et al.

www.manaraa.com